Submitted to the XVIth
International Conference on
High Energy Physics, Batavia,
Ill., Sept. 6-13, 1972

LBL-1020

STRUCTURE IN THE $2\pi^0$ MASS SPECTRUM IN THE REACTION $\pi^- p \to n\pi^0\pi^0$ AT 1.6 TO 2.4 GeV/c

A. Skuja, M.A. Wahlig, T.B. Risser, M. Pripstein,
J.E. Nelson, I.R. Linscott, R.W. Kenney,
O.I. Dahl, and R.B. Chaffee

July 1972

AEC Contract No. W-7405-eng-48

LBL-1020

DISCLAIMER

Submitted to the XVIth International Conference on High Energy Physics, Batavia, Ill., Sept. 6-13, 1972

LBL-1020

STRUCTURE IN THE $2\pi^0$ MASS SPECTRUM IN THE REACTION $\pi^- p \to n\pi^0\pi^0$ at 1.6 to 2.4 GeV/c*

A. Skuja,† M. A. Wahlig, T. B. Risser,‡ M. Pripstein, J. E. Nelson

I. R. Linscott, R. W. Kenney, O. I. Dahl and R. B. Chaffee+

Lawrence Berkeley Laboratory
University of California
Berkeley, California

July, 1972

ABSTRACT

We report results from a study of the reaction $\pi^- p \to n\pi^0\pi^0$ between 1.6 and 2.4 GeV/c, in which all the final-state particles were detected using a 3.7 π-steradian array of optical spark chambers and shower-counters and a set of 20 neutron counters subtending a polar lab angle region of 12 to 72 degrees. The most prominent feature of the reaction at low four-momentum-transfer, t, to the nucleon, is $\Delta(1236)$ production. The $2\pi^0$ mass spectrum at low t [< 0.3 $(\text{GeV/c})^2$], with $\Delta(1236)$ events removed, exhibits a marked enhancement with respect to peripheral phase space in the region above 700 MeV. The quantum numbers for the observed structure are consistent with T = 0, J = 0. We have parameterized the enhancement in two ways: 1) as a Breit-Wigner shape resonance, which gives an acceptable fit to the data with a fitted mass of 820 $\pm$ 15 MeV and width of 220 $\pm$ 60 MeV, and 2) in terms of the One-Pion-Exchange model modified by the Dürr-Pilkuhn form factor. The data completely rule out the so-called "down-up" solution.

*Work done under the auspices of the U. S. Atomic Energy Commission

†Present Address: Nuclear Physics Laboratory, Oxford University, Keble Road, Oxford England

‡Present Address: CEN Saclay, B. P. No. 2, 91 Gif-Sur-Yvette, France. Address after September 1: Physics Department, University of California at Santa Barbara, Santa Barbara, California 93106

+Present Address: Stanford Linear Accelerator Center, Stanford University, Stanford, California 94305.

Since the discovery of the persistent "forward-backward" asymmetry in the decay of the peripherally produced neutral ρ (765) meson, the commonly accepted explanation of this asymmetry is interference between the isotopic spin T = 1, angular momentum J = 1 ρ amplitude and a T = 0, J = 0 π-π amplitude whose phase, $\delta_o^o (= \delta_J^T)$, is near $\pi/2$ at energies close to the ρ mass. Beyond this, however, there has been much speculation and controversy over the detailed properties of δ_o^o, particularly below 1 GeV in π-π invariant mass.[1] Most of the analyses[1] of δ_o^o have come from studies of the π^+-π^- system in the reactions

$$\pi^- + p \rightarrow n + \pi^+ + \pi^- \qquad (1)$$

and

$$\pi^+ + p \rightarrow \Delta^{++}(1236) + \pi^+ + \pi^- \qquad (2)$$

The dominant ρ production, coupled with possible non-one-pion-exchange contributions, has made it difficult to extract a unique set of δ_o^o phase shifts from threshold to about 1 GeV in π-π mass.

A more sensitive approach, albeit more difficult experimentally, is to study the reaction

$$\pi^- + p \rightarrow n + \pi^o + \pi^o \qquad (3)$$

in which ρ production is forbidden. Although the dipion system in reaction (3) can have T = 2 as well as T = 0, previous studies of the $\pi^+\pi^+$ and $\pi^-\pi^-$ systems indicate that there is no structure in the T = 2 dipion system below 1 GeV and that the T = 2 phase shift δ_o^2 is small everywhere in this region.[2] Thus, any structure in the $2\pi^o$ system may be attributed to the T = 0 state.

We have performed an experiment at the Berkeley Bevatron to study reaction (3), $\pi^- p \rightarrow n\pi^o\pi^o$, at beam momenta of 1.59 to 2.39 GeV/c in 0.20-GeV/c intervals. The salient features of the experiment are, 1) a very

high probability for detecting γ-rays using a large cubic array of lead-plate optical spark chambers and 2) identification of the final state by detecting the neutron (both its angle and time-of-flight) and all the γ-rays from the π^o-decays, measuring the kinematic variables of each of the particles and making a highly over-constrained kinematic fit of the data (6-constraint-3-vertex-fit) using a modified version of the LBL Group A bubble chamber program (SIOUX).[3] Another important feature is that prominent systematic effects were empirically calibrated during the course of the experiment by also collecting data on the two-body reactions

$$\pi^- p \rightarrow n\pi^o \quad (4)$$
$$\qquad\qquad\quad \hookrightarrow 2\gamma$$

and

$$\pi^- p \rightarrow n\eta \quad (5)$$
$$\qquad\qquad\quad \hookrightarrow 2\gamma$$

with and without the neutron counters in the triggering logic and comparing the results from these two sets of running conditions. This eliminated the necessity of relying primarily on Monte-Carlo calculations to assess these systematic effects.

A schematic diagram of the experimental layout is shown in Fig. 1. A detailed description of all the apparatus and its performance characteristics is given in Refs. 4 and 5. The π^--beam from the Bevatron had a momentum bite, $\Delta p/p = \pm 1\%$, and was focused to a spot size of 1.5-in. horizontally by 0.75-in. vertically (FWHM) at a liquid hydrogen target, 8-in. long by 4-in. diameter. Counter hodoscopes defined the beam direction at the target to within $\pm$ 0.2 deg (rms). The target was surrounded by anti-coincidence counters, A_1 and A_2, which vetoed any interaction in which charged particles were produced. A neutral-final-

state trigger was defined by a coincidence of a 3-counter beam telescope, $M_1M_2M_3$, and the anti-counters, i.e., $M_1M_2M_3\bar{A}_1\bar{A}_2$. The beam contamination of μ^- and e^- was monitored by a threshold Cerenkov counter. The γ-rays were detected by a large cubic array of lead-plate optical spark chambers [4-6] surrounding the target and covering five sides of a cube, with the sixth side (beam entrance face) almost completely covered by shower counters of lead-scintillator sandwiches (G_i in Fig. 1). As a result, the lab solid-angle subtended for γ-ray detection was 3.7 π steradians. Each of the four side chambers was ~ 7 radiation lengths thick, consisting of 42 thin lead plates and 12 aluminum plates of dimension 4 by 5 feet. The downstream chamber was ~ 8 radiation lengths thick, made up of 48 lead and 13 aluminum plates, 6.5 ft. square. Each lead plate consisted of a lamination of 1/32-in. lead between two sheets of 1/64-in. aluminum. The plates were made very thin in order to ensure a high detection efficiency for low energy showers. The γ-ray detection threshold was about 10 MeV, and the average detection probability was 89% per γ-ray,[4] averaged over all γ-ray energies and production lab angles for γ's produced in multi-pion final states.[7] The first four gaps in each chamber had aluminum plates 3/64-in. thick and were used as a visual veto for any charged particles which managed to enter the chambers. Each of the five chambers was photographed in two orthogonal views for 90-deg stereo, with the 10 views made visible to a single camera by means of a system of 46 mirrors.

The neutron detector consisted of 20 thick plastic-scintillator counters. Each scintillator was a cylinder 8-in. in diameter and 8-in. thick, viewed on axis by an Amperex XP-1040 phototube. Each neutron counter had an additional counter mounted in front of it to veto charged

particles. The neutron counters were placed side-by-side, along an arc of a circle approximately 15 ft. in radius with the hydrogen target as a center. The counters subtended a polar lab angle interval of 12 to 72 deg with respect to the central beam ray. For neutron kinematic energies above 20 MeV ($\beta \gtrsim 0.2$) the average neutron detection efficiency of these counters was $20 \pm 2\%$ and did not vary much with energy. For lower energy neutrons, the detection efficiency dropped rapidly. To avoid possible biases in the data due to uncertainties in the rapid variation of detection efficiency, a cut-off in the neutron timing gate was set so that no neutron of $\beta < 0.17$ would be accepted. In addition, to avoid being flooded by γ-ray triggers, the neutron counter timing gate was adjusted to eliminate any triggers in a time-of-flight interval corresponding to $\beta \geq 0.84$.[4,8] Figure 2 shows the neutron kinematics for the reaction $\pi^- p \rightarrow n$ + missing mass at 2.4 GeV/c, and the region covered by the neutron counters in our timing gate. The neutron counter (zero-crossing) timing resolution, $\pm$ 0.6 ns, was determined by measuring the time-of-flight of mono-energetic neutrons produced in the charge-exchange reaction (4) at small lab angles. The time-of-flight spectra were continuously monitored during the course of the experiment.

Data were collected with and without the neutron counter coincidence in the event trigger. More specifically, in the former case the trigger consisted of a neutral-final-state coincidence $M_1 M_2 M_3 \bar{A}_1 \bar{A}_2$ in coincidence with a neutron counter signal occurring within the timing gate (corresponding to $\beta_n = 0.17 - 0.84$). When these conditions were met, the spark chambers were triggered and the event was photographed, with the neutron counter information and that from the beam hodoscope and shower counters

(G_i) recorded on an array of lights on a data-box which was also photographed. For both sets of running conditions, the target-empty trigger rate was between 11 and 16% of the target-full rate, depending on the beam momentum.

The film was scanned by a group of scanners who recorded the number of showers, the location of the first spark of each shower within a scanning grid-zone corresponding to 2 in. in real space, and information about non-shower tracks (e.g., beam tracks) in the chambers. The film was measured on the LBL SASS machine[9]--a precision cathode ray tube and photomultiplier system linked to a DDP-24 computer. SASS digitizes the position of all sparks, fiducial lights, and data box lights for each event. The information was then processed through a pattern recognition program which uses the scanners' information on the first spark position and the number of showers as a guide in reconstructing accurately the shower geometry in three-dimensional space. The γ-ray energy resolution from spark counting was calibrated with "tagged" γ's from an over-constrained kinematic fit of 2-shower events to reactions (4) and (5), using the neutron-counter information and the measured directions of the γ's in the fit.[10] Scanning efficiency for each γ-ray multiplicity was determined by having the scanners triple-scan about 9,000 frames, with a physicist doing the conflict (fourth) scan of the data.[11]

The neutral-final-state-trigger data was used to determine the total $\pi^- p \to$ neutrals cross-section and the partial cross-sections for $\pi^- p \to n + M\,\gamma$'s ($M = 0, \ldots, 8$). This data, unlike the neutron-counter-trigger data, did not have the drawback of any severe geometric or kinematic cuts. Moreover, the procedure was free from most systematic

biases, such as neutron-Pb scattering in the spark chambers, γ-ray measuring resolution, etc. The partial cross-sections were determined by counting the number of events of each γ-ray multiplicity observed by the scanners and applying known corrections for detection inefficiencies. A detailed description is given in Ref. 4 and the corrections are summarized in footnote 12 below. The partial cross-section for the corrected 4-γ final state is then assumed to be that for $n\pi^o\pi^o$. It is shown in Fig. 3, along with the total neutral cross-section, as a function of beam momentum. The largest contribution to the errors on the cross-sections comes from our conservative estimate of the uncertainty in the average γ-ray detection probability. Partial cross-sections for the other final states are reported elsewhere.[4,13] Results from other experiments[14-17] are shown in Fig. 3. It is seen that our cross-sections for $n\pi^o\pi^o$ agree very well with those of Crouch et al.[16] but are about twice as large as those of Carroll et al.[15]

The study of the dynamical properties of reaction (3), $\pi^- p \to n\pi^o\pi^o$, was made with the neutron-counter-trigger data sample containing four visible showers in the chambers and no upstream shower-counter signal. Before presenting results, we first describe the calibration of the important systematic effects. As is shown in Fig. 1, neutrons produced in the target had to pass through the spark chambers and therefore a fraction (~25 to 30%) of them would undergo inelastic scattering from n-Pb and n-Al interactions.[18a] This effect had two consequences: 1) it attenuated the flux of neutrons originally produced at the target in the "good" direction of a neutron counter and 2) it caused neutrons produced in a so-called "bad" direction (i.e., pointing away from the counters) to

be scattered into the counters. On the average, the number of fast neutrons ($\gtrsim$ 20 MeV) produced in n-Pb + n-Al inelastic collisions is about two at these energies,[18] which means that there were about twice as many neutron-counter triggers caused by "bad" neutrons scattering into the counters as there were by "good" neutrons scattered away from the counters. This could pose a serious problem for neutron missing-mass experiments which use spark chambers to isolate the 4-shower $n\pi^o\pi^o$ final state.[19] These "bad" neutron triggers can be eliminated by making an over-constrained kinematic fit of the 4-shower data to the $n\pi^o\pi^o$ hypothesis and rejecting the events with poor χ^2. The correction due to the attenuation of the "good" neutrons is, in principle, calculable since the n-Pb and n-Al inelastic cross-sections are known as a function of neutron kinetic energy.[18] We have written a Monte-Carlo program, incorporating these cross-sections, which calculates the scattering of neutrons in the chambers as a function of their energy, position, and direction. This was empirically checked using the 2-shower events obtained in both triggering modes (i.e., with and without neutron coincidence in the final trigger) at various momenta. The events were fit to the 2-body hypotheses, reactions (4) and (5), and the differential cross-sections calculated, with the fitted events from neutron-counter-trigger data being corrected for neutron detection efficiency, counter geometry, and neutron attenuation in the spark chambers as calculated in the Monte-Carlo program. Within the kinematic region defined by the neutron-counter timing gate and lab angle interval shown in Fig. 2, the differential cross-sections agree everywhere to within 10%. A further study of 2- and 4-shower events, taken with the neutron-counter-trigger,

indicates that almost all "bad" neutron-trigger events can be eliminated in the 4-shower events by rejecting all events with χ^2 = probability of less than 5%. This is the cut for all data to be discussed from here on.

The mass resolution of the neutron-counter-trigger data is determined primarily by the neutron angle and time-of-flight information. This was calibrated by fitting the 2-shower events to the hypothesis, $\pi^- p \rightarrow n + \gamma + \gamma$. The γ-γ mass spectrum, combining the data from all five beam momenta together, is shown in Fig. 4. Two large peaks, corresponding to the π^o and η masses, are clearly visible above a very small (10%) background. The events have been weighted to correct for neutron scattering in the chambers, neutron counter geometry and detection efficiency.[20] The average weight is ~ 1.5. The same weights are also applied to the 4-shower data. As seen from Fig. 4., the mass resolution (HWHM) is approximately $\pm$ 20 MeV at the π^o mass and $\pm$ 35 MeV at the η mass.[21]

In the data sample reported here, there are about 7,400 unweighted events within our timing gate that fit the $n\pi^o\pi^o$ reaction (3), with χ^2-probability > 5%. The timing gate width defines the invariant four-momentum-transfer, $t_{p \rightarrow \eta}$, to be between 0.029 and 1.54 $(GeV/c)^2$. The neutron production distribution is peaked at low t. Cross-sections were determined by normalizing this data to the total $n\pi^o\pi^o$ cross-sections obtained from the neutral-final-state-trigger data[22] as outlined in Ref. 4. The cross sections for $t \leq 0.3$ $(GeV/c)^2$ are given in Table I.

Figure 5 shows the mass spectra for the $\pi^o\pi^o$ and $n\pi^o$ systems for t from 0.029 to 0.3 $(GeV/c)^2$ (~ 2900 events). The dominant features are the peak in the $n\pi^o$ spectrum corresponding to $\Delta(1236)$ production and a lower but broader secondary peak corresponding to its reflection since

both $n\pi^o$ combinations are plotted. In order to investigate the dynamical properties of the $2\pi^o$ system free from the effects due to $\Delta(1236)$, we cut out the Δ events by removing all events having at least one $n\pi^o$ combination in the broad mass band 1100 to 1300 MeV. The $n\pi^o$ mass spectrum of the surviving events (not shown) exhibits no resonant structure. At low t, the t distribution for events with Δ cut out is essentially independent of $\pi^o\pi^o$ mass below approximately 1 GeV.

To study quantitatively the peripheral $2\pi^o$ production, we tried various parameterizations of the data using the LBL maximum likelihood fitting routine OPTIME.[23] This program generated a set of Monte-Carlo events for the $n\pi^o\pi^o$ final state according to phase space, incorporating the geometry of our detectors and the same kinematic cuts (such as neutron timing gate width, Δ cuts, etc.) as were applied to the data. The data parameterization procedure consists of weighting these Monte-Carlo events by a matrix element corresponding to the hypothesis or model being tested, with the weighted events then used in the maximum likelihood fit to the data. We first parameterized the data by fitting the t distribution with a phase space distribution modified by a t-dependent form factor. A comparison of the predicted $\pi^o\pi^o$ mass spectrum resulting from this matrix element with the data indicated that additional parameterization was necessary, as discussed below

Figure 6 shows the t distribution for $M_{\pi^o\pi^o} < 1$ GeV, with the Δ-band events excluded. For each beam momentum, the low-t distribution is more peripheral than phase space multiplied by the one-pion-exchange (OPE) propagator, $\frac{1}{(t + \mu^2)^2}$, where μ is the pion mass. To parameterize the observed distribution at each momentum, we multiplied the OPE propagator

by a form factor. Two form factors were tried: 1) a single exponential,[4] $e^{-a(t + \mu^2)}$ and 2) the phenomenological Dürr-Pilkuhn[24] vertex factor multiplied by Wolf's t-dependent form factor,[25] which for S-wave scattering is

$$F(t) = \left(\frac{2.3 - \mu^2}{2.3 + t}\right)^2 \cdot \left(\frac{1 + 2.66^2 q_n^2}{1 + 2.66^2 q_t^2}\right) \qquad (6)$$

where $(q_t)^2$ is the momentum squared of the incoming target proton evaluated in the neutron rest system, and q_n^2 is this quantity taken on-shell. Both form factors yielded acceptable fits to the data for a very small t region. However, the latter describes the production distribution better over a wider range of t-values, $\left[\text{to } t \leq 0.3 \text{ (GeV/c)}^2\right]$ than does a single exponential. Hence we use it. The curve in Fig. 6 is the sum over the five beam momenta, of the expression $\left[F(t) \cdot \frac{t}{(t + \mu^2)^2} \cdot (\text{phase space})\right]$, normalized to the number of events with $t \leq 0.3$ (GeV/c)^2 at each momentum. We henceforth refer to this expression as "peripheral phase space."

Figure 7 shows the $\pi^o\pi^o$ mass spectrum for $t \leq 0.3$ (GeV/c)^2 with events in the Δ-mass band rejected (= 1323 events). The solid curve represents peripheral phase space, normalized to the data below 1000 MeV but outside the 700 to 900 MeV region. The curve and the data agree quite well except in the region $M_{\pi^o\pi^o} \approx 660$ to 940 MeV where the data exhibits a marked enhancement over peripheral phase space. In accordance with our introductory remarks, this enhancement may be attributed to a T = 0 π-π interaction. To determine the angular momentum of this enhancement, we studied the dipion decay distribution with respect to the incident π^- direction in the dipion rest frame. For all $2\pi^o$ masses below 1000 MeV,

the decay distribution was consistent with isotropy outside the region corresponding to the Δ-mass-band cut. If we assume one-pion-exchange (OPE) for the dipion production mechanism, then the absence of structure in this decay distribution implies that the $2\pi^o$ system is S-wave.

We have parameterized the $2\pi^o$ mass spectrum in two ways: 1) We characterize the enhancement as a Breit-Wigner and fit the data to an expression of the form $\left\{(\text{peripheral phase space})\left[a + b(\text{Breit-Wigner})\right]\right\}$, allowing the mass and width of the Breit-Wigner to be free parameters. We get an acceptable fit (χ^2 - probability $\approx 15\%$) with a mass of 820 $\pm$ 15 MeV and width of 220 $\pm$ 60 MeV for the Breit-Wigner term. 2) We assume OPE production and use the Chew-Low equation,[26] modified by the form factor F(t) above, and work in the physical region (but replacing the "off-shell" pion momentum by the "on-shell" momentum). The formula used, relating the "off-shell" cross section, $d^2\sigma/dM_{\pi\pi}dt$ to the "on-shell" cross-section, $\sigma_{\pi\pi}$ in the S-wave approximation, is

$$\frac{d^2\sigma}{dM_{\pi\pi}dt} = \frac{1}{4\pi M^2 P_L^2} \frac{t}{(t+\mu^2)^2} \frac{g^2}{4\pi} M_{\pi\pi}^2 \, q\sigma_{\pi\pi} \cdot F(t) \qquad (7a)$$

and

$$\sigma_{\pi\pi} = \frac{4\pi}{q^2} \frac{2}{9} \sin^2(\delta_o^o - \delta_o^2) \qquad (7b)$$

where M = proton mass

P_L = lab beam momentum

$g^2/4\pi = 29.2$

$\delta_o^o(\delta_o^2)$ is the T = 0 (T = 2) S-wave phase shift and q is the pion momentum in the dipion rest frame.[27] The term $\sin^2(\delta_o^o - \delta_o^2)$ was evaluated at each beam momentum as a function of $M_{\pi\pi}$. A weighted average for all the beam

momenta is plotted in Fig. 8a. The error bars in each bin include the statistical errors of the data and of the Monte-Carlo events as well. The uncertainty in the overall normalization (within $\pm$ 10%) of our data[22] is not included. For comparison we plot the predictions from the recent T = 0, S-wave phase-shift solutions of Protopopescu et al.,[28] using T = 2 phase-shifts of Baton et al.[29] It is evident that the so-called "down-up" solution above the ρ mass is clearly in disagreement with the data and can be ruled out completely--a conclusion consistent with that of Ref. 28. The prediction of the down-down solution is much closer qualitatively to the data.

To facilitate the comparison further we have eliminated the effect of the small uncertainty in our overall normalization as follows. We introduced the phase shifts of Refs. 28 and 29 into our Monte-Carlo and generated the $\pi^o\pi^o$ mass spectrum at each beam momentum, subject to the same geometric and kinematic cuts as were applied to the data. The resulting spectrum was then normalized to the number of events in the data with $\pi^o\pi^o$ mass between 400 and 940 MeV. The data and the Monte-Carlo events from all the momenta were then combined and are shown in Fig. 8b. The data are the same as in Fig. 7. The disagreement between the data and the down-down solution may be due to δ_o^2 or δ_o^o being somewhat different from the values derived in the solutions of Refs. 29 and 28, or it may be due to possible non-OPE contributions in our data.

We wish to thank Dr. Sherwood Parker and Dr. Charles Rey for their care and great skill in constructing a fine set of spark chambers and the Bevatron crew for extending the art of accelerator operation to provide us very smooth beam conditions. We also wish to express our

appreciation to Mr. Robert Hogrefe, Ms. Ellen Epstein and our group of scanners for their diligent efforts. It is a pleasure to acknowledge the constant moral and intellectual support provided by the members of Group A and the Moyer-Helmholz groups at LBL. Lastly, we wish to thank Mr. Serban Protopopescu and Drs. Tom Lasinski and Eugene Colton for fruitful discussions about π-π scattering.

REFERENCES

1. For a review of the T = 0, J = 0 π-π system, refer to:
(a) M. Derrick, Proc. of the Boulder Conference on High Energy Physics, p. 291 (1969)
(b) D. Morgan and J. Pisut, Springer Tracts in Modern Physics, 55 (1970)
(c) J. L. Petersen, Physics Reports 2C, 157 (1971)
(d) Proc. of the Argonne Conference on $\pi\pi$ and Kπ Interactions (1969).

2. N. Armenise et al., Nuovo Cimento 37, 361 (1965); E. Colton, E. Malamud, P. E. Schlein, A. D. Johnson, V. J. Stenger and P. G. Wohlmut, Phys. Rev. D, 3, 2028 (1971).

3. O. I. Dahl, T. B. Day, F. T. Solmitz and N. L. Gould, LBL Group A Programming Note No. P-126 (unpublished).

4. Andris Skuja, "Study of Dipion Production in the Reaction $\pi^- p \rightarrow \pi^o \pi^o n$ Between 1.6 and 2.4 GeV/c (Ph. D. thesis) (1972).

5. Thomas Bard Risser, "Neutral Decays of the η^o Meson" (Ph. D. thesis) (1970).

6. R. J. Cence, B. D. Jones, V. Z. Peterson, V. J. Stenger, J. Wilson, D. Cheng, R. D. Eandi, R. W. Kenney, I. Linscott, W. P. Oliver, S. Parker, and C. Rey, Phys. Rev. Letters 22, 1210 (1969); C. A. Rey and S. I. Parker, Nucl. Inst. Meth. 54, 314 (1967) and 43, 361 (1966).

7. Because of the dynamics of the charge-exchange reaction, $\pi^- p \rightarrow n\pi^o$, the detection probability was 94% per γ-ray for this reaction.

8. "Early-time" triggers (i.e., for times-of-flight corresponding to unphysical $\beta > 1.2$) were also accepted and the events were used to study the low room background.

9. A. R. Clark, L. T. Kerth, Proc. of the 1966 Conference on Instrumentation for High Energy Physics, Stanford, California, p. 355 (1966).

10. For $E_\gamma \lesssim 300$ MeV, the energy resolution, $\Delta E_\gamma / E_\gamma \approx \pm 40\%$ and became progressively worse to $\Delta E_\gamma / E_\gamma \approx \pm 100\%$ at $E_\gamma \approx 1$ GeV. Even the poor resolution at 1 GeV was useful in resolving ambiguities in the kinematic fit.

11. This is a larger data sample than used in Ref. 4 and therefore provided smaller errors on the scanning efficiencies. The scanning efficiencies are essentially the same as in Ref. 4.

12. The corrections, in the order applied to the raw data, are: 1) Target empty subtraction (0.11 to 0.13 depending on momentum), 2) Scanning efficiency matrix (average efficiency for 2- and 4-shower events was 0.94 ± 0.02 and 0.86 ± 0.02, respectively), 3) Feed-up due to presence of a shower from a previous event which is still visible because of the long active time of the chambers ($= 0.04 \pm 0.02$ for 1-shower feed-up and $0.01 \pm .01$ for 2-shower feed-up). This correction is applied to each final-state γ-multiplicity; 4) detection probability, due to γ's not converting in the chambers or escaping through the beam entrance hole causing feed-down ($= 0.89 \pm 0.01$ per γ-ray); 5) Vetoes of bona-fide events due to a) γ-ray conversion in the target or anti-counters ($= 0.02 \pm .005$ per γ-ray), b) Dalitz-pair conversion ($= 0.0116$ per π^o), c) neutron interaction in the target and anti-counters ($= 0.011$) and d) δ-rays produced by incident π^- ($= 0.015 \pm .005$); 6) Beam contamination of μ^- and e^- ($= 0.11 \pm 0.01$).

13. J. E. Nelson, (Ph. D. thesis) LBL-1019 (1972).

14. G. Bizard, Y. Declais, J. Duchon, J. L. Laville, J. Seguinol,

C. Bricman, J. M. Peireau, C. Valladas, Physics Letters 31B, 481 (1970).

15. A. S. Carroll, I. F. Corbett, C. J. S. Damerell, N. Middlemas, D. Newton, A. B. Clegg and W. S. C. Williams, Phys. Rev. 177, 2047 (1969).

16. H. R. Crouch et al., Phys. Rev. Letters 21, 845 (1968).

17. M. Feldman et al., Nuovo Cimento LA 89 (1967).

18. Elastic scattering from such heavy nuclei hardly perturbs the neutron and is essentially unnoticeable within the resolution of our neutron counters.

18. S. J. Lindenbaum, Ann. Rev. Nucl. Science 11, 213 (1961); N. Metropolis, R. Binns, M. Storm, J. M. Miller, G. Friedlander, Phys. Rev. 110, 204 (1958).

19. M. Deinet, A. Menzione, H. Muller and H. M. Staudenmauer, S. Buniatav and D. Schmitt, Physics Letters 30B, 359 (1969).

20. This corrects for the slight variation in neutron detection efficiency as a function of kinetic energies accepted within the timing gate.

21. According to our Monte-Carlo, the mass resolution hardly varies above the η mass.

22. A study of the resolution of the data taken in both triggering modes indicates that this procedure yields the correct neutron-counter-triggered cross-sections to within an uncertainty of $\pm$ 10%.

23. P. H. Eberhard and W. O. Koellner, UCRL-20159 (1970), and UCRL-20160 (1971).

24. H. P. Dürr and H. Pilkuhn, Nuovo Cimento 40, 899 (1965).

25. G. Wolf, Phys. Rev. Letters 19, 925 (1967), and Phys. Rev. 182, 1538 (1969).

26. G. F. Chew and F. E. Low, Phys. Rev. 113, 1640 (1959).

27. In the determination of $\sigma_{\pi\pi}$ in Ref. 4, the off-shell pion momentum was used in the expression corresponding to (7), instead of the on-shell momentum, q. This reduced $\sigma_{\pi\pi}$ by about 30%.

28. S. D. Protopopescu, M. Alston-Garnjost, A. Barbaro-Galtieri, S. M. Flatte, J. H. Friedman, T. A. Lasinski, G. R. Lynch, M. S. Rabin and F. T. Solmitz, Proc. of the 1972 International Conference on Meson Spectroscopy, Philadelphia, Pa., April 28-29, 1972 (to be published) and LBL-787. Below 780 MeV they are the same as those of Baton et al. reported in Ref. 29.

29. J. P. Baton, G. Laurens and J. Reignier, Physics Letters 33B, 528 (1970)

Table I. Cross-Sections

P_{π^-} (GeV/c)	$\pi^- p \to n\pi^o\pi^o$ (μb)	$\pi^- p \to n\pi^o\pi^o$ for $0.029 \leq t \leq 0.3$ $(GeV/c)^2$, $\Delta(1236)$ contribution removed.* (μb)
1.59	1310±80	325±31
1.79	1360±80	432±36
1.99	1390±80	337±30
2.19	1380±80	316±27
2.39	1140±60	226±17

*The $\Delta(1236)$ contribution was removed by cutting out all the events in the $\Delta(1236)$ mass band and correcting for the fraction of phase space that had been removed.

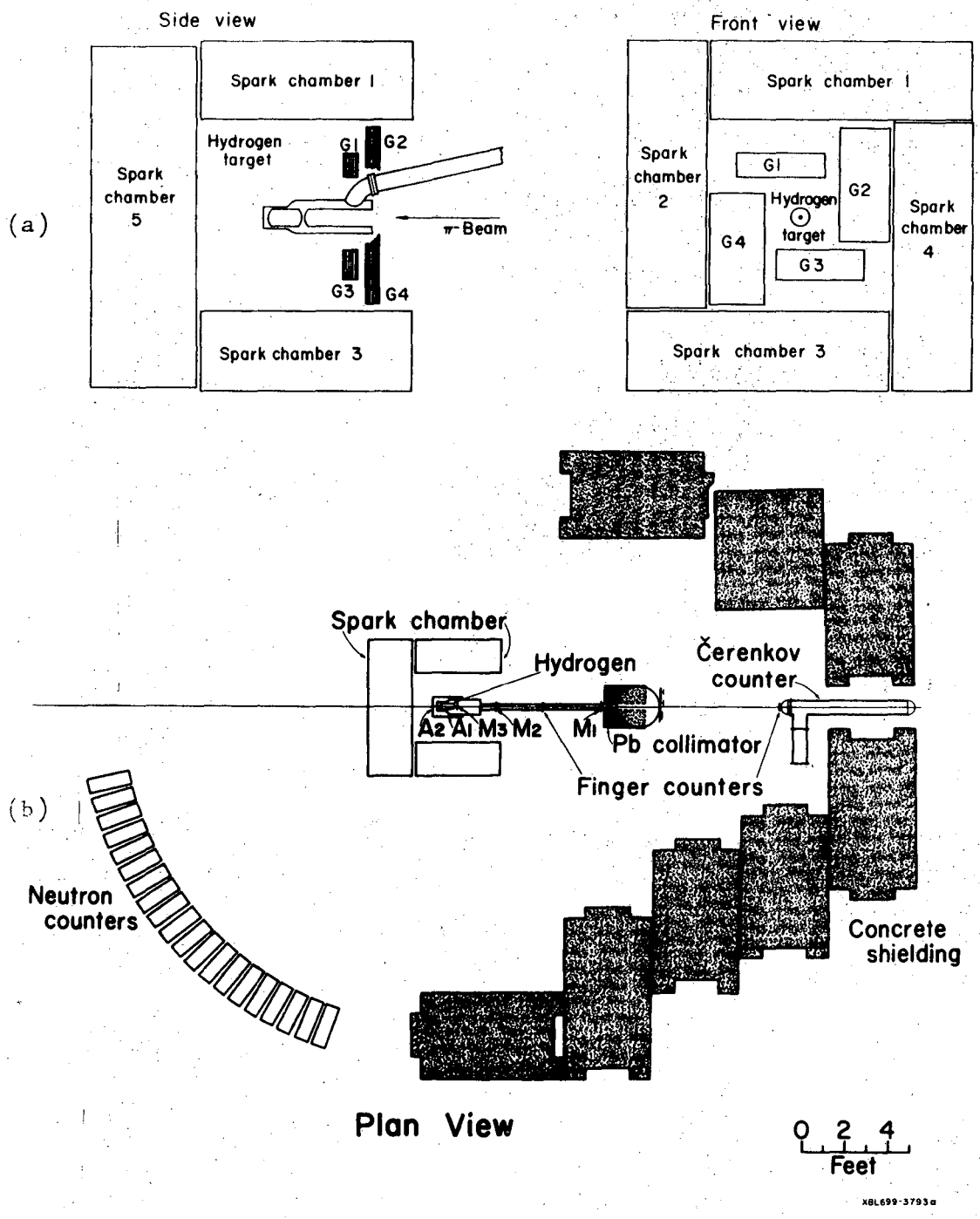

Fig. 1. Layout of the apparatus: (a) arrangement of spark chambers, hydrogen target and γ-ray detection counters (G_i), and (b) plan view of entire layout.

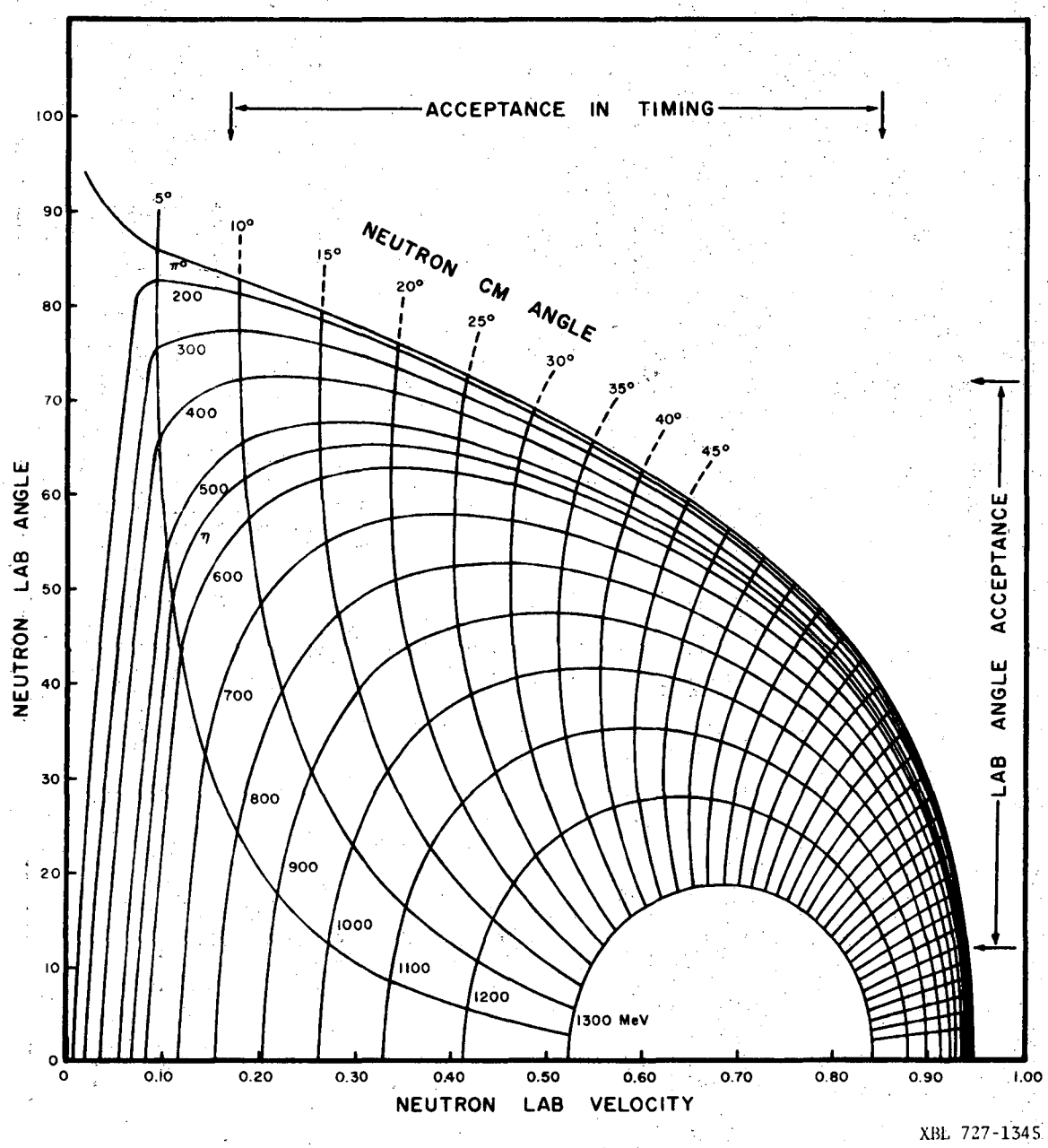

XBL 727-1345

Fig. 2. Kinematics for the reaction $\pi^- p \rightarrow nX^-$ at an incident π^- momentum of 2.4 GeV/c.

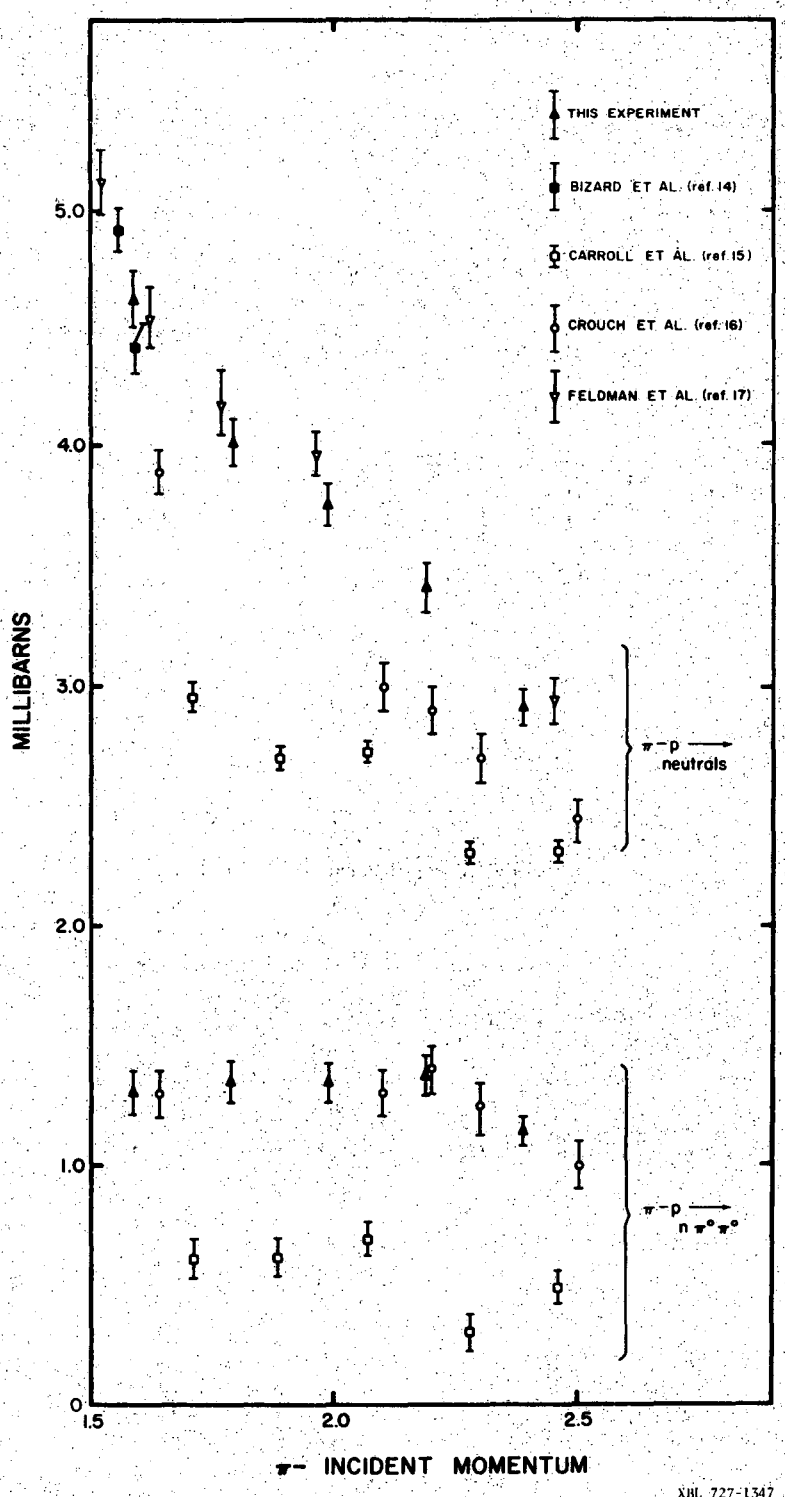

Fig. 3. Cross sections for $\pi^- p \rightarrow$ neutrals and $\pi^- p \rightarrow n\pi^o\pi^o$.

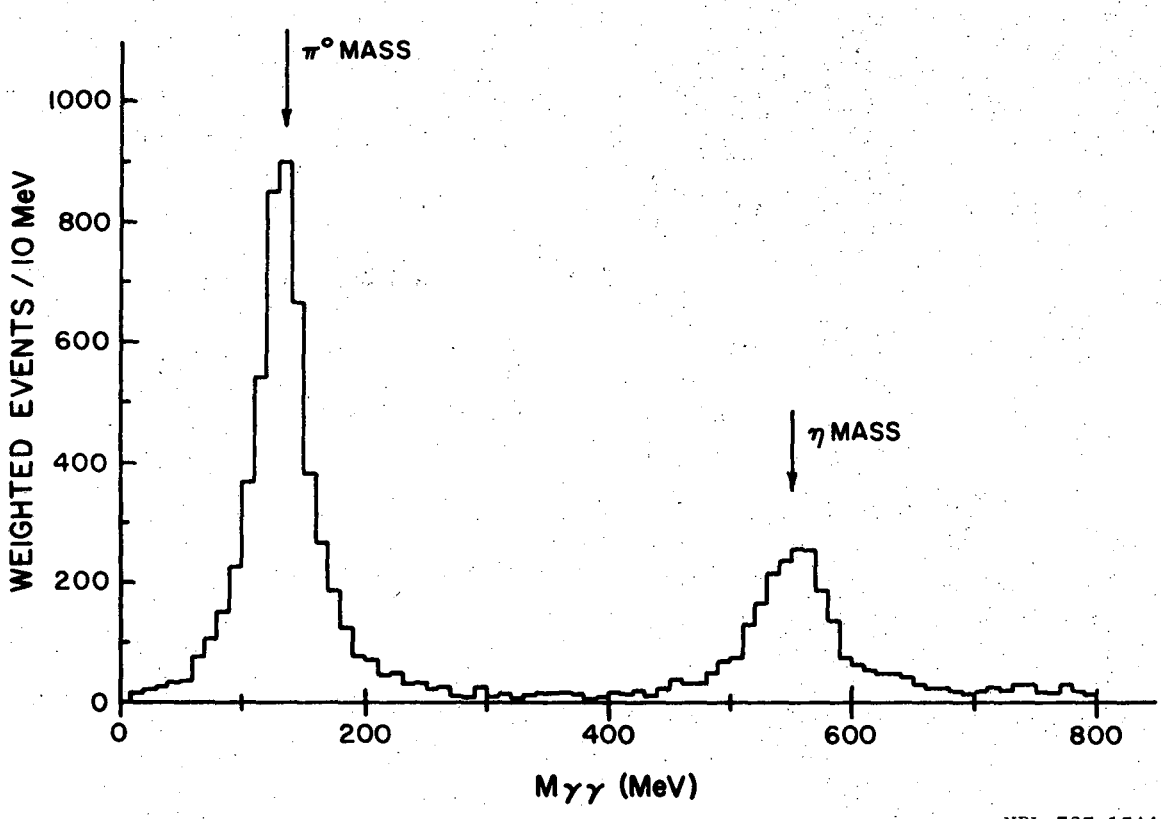

XBL 727-1344

Fig. 4. Di-gamma mass spectrum from 2-shower events fitting the reaction $\pi^- p \rightarrow n\gamma\gamma$. This is the neutron-counter-trigger data from all five π^- beam momenta combined.

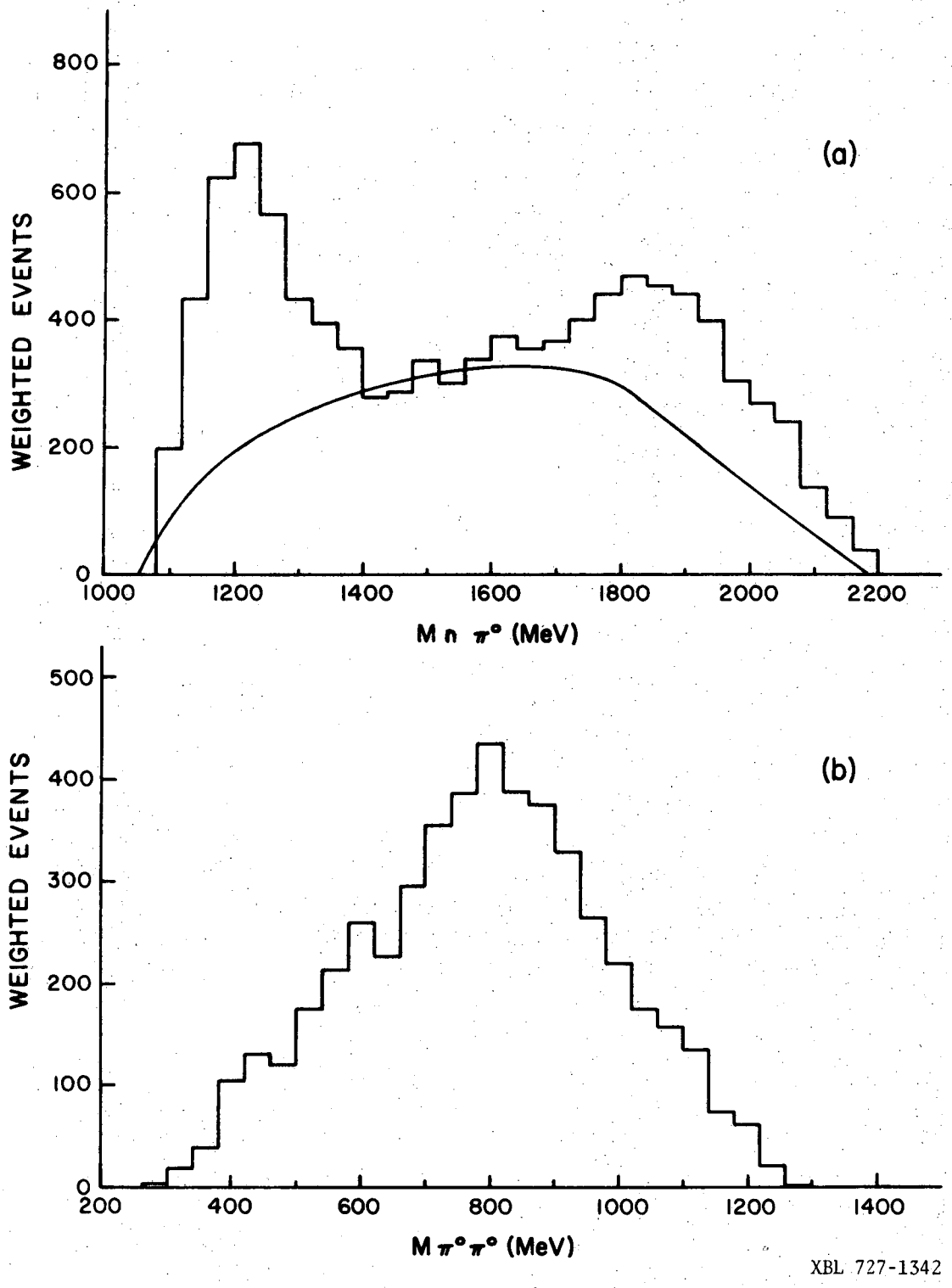

Fig. 5. Mass spectra of (a) $n\pi^o$ and (b) $\pi^o\pi^o$ from the reaction $\pi^- p \to n\pi^o\pi^o$ for $0.029 \leq t \leq 0.3$ $(GeV/c)^2$. Data are from all five momenta. The curve represents phase space, arbitrarily normalized.

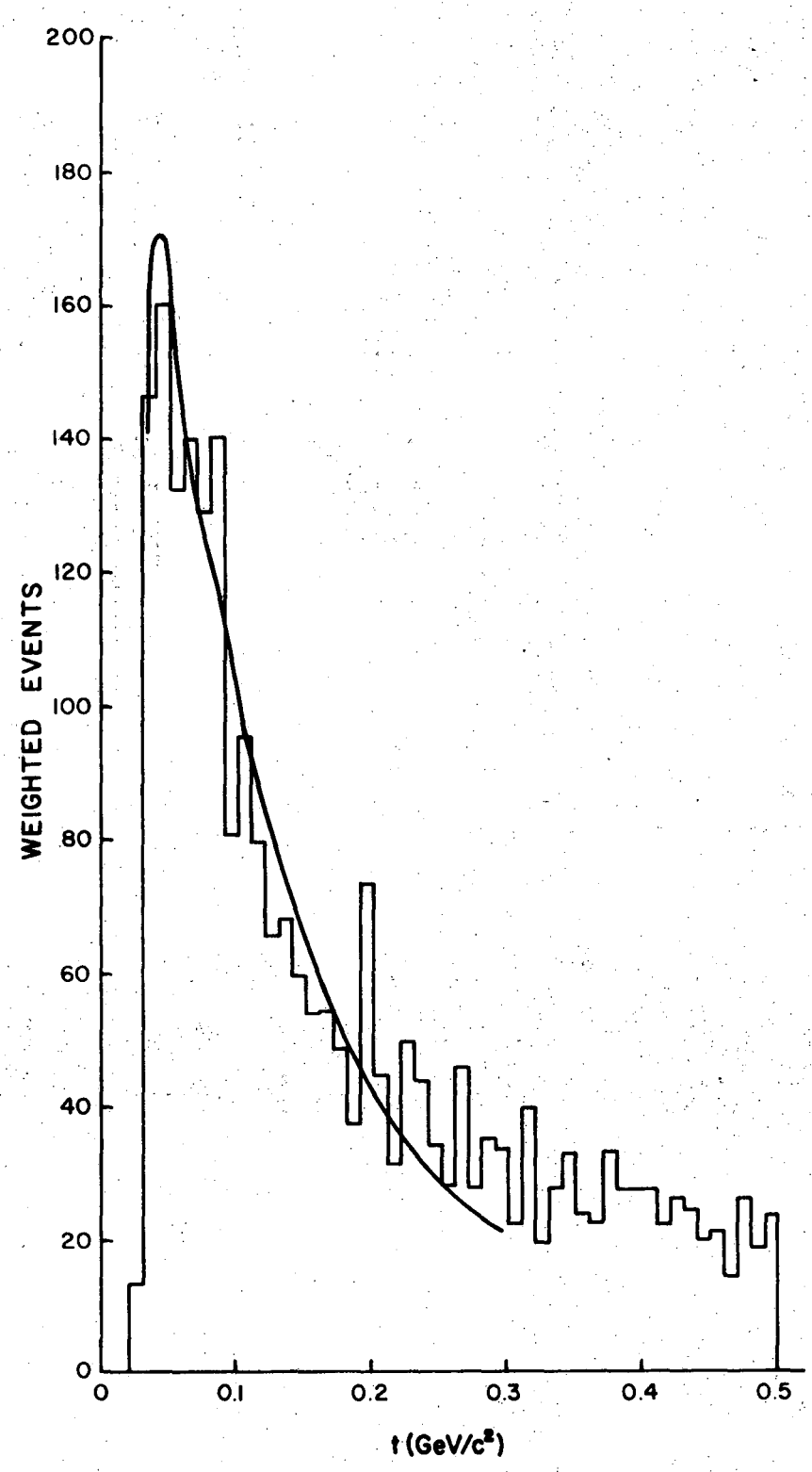

XBL 727-1346

Fig. 6. Four-momentum-transfer distribution, $t_{p \to n'}$ for $M_{\pi^o\pi^o} < 1$ GeV and Δ-band events excluded. Combined data from all beam momenta. The curve in $\left[F(t) \cdot \left(t/(t + \mu^2)^2\right) \cdot (\text{phase space})\right]$ normalized to the data as described in the text.

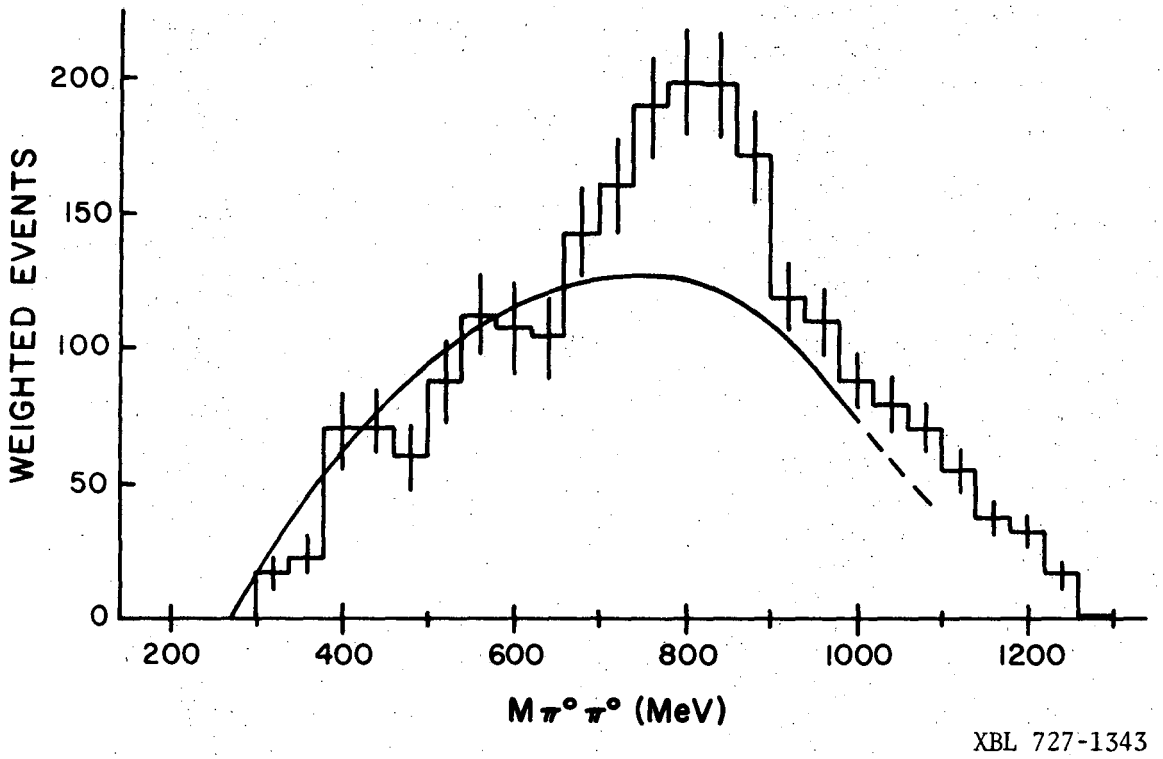

XBL 727-1343

Fig. 7. Mass spectrum of $\pi^0\pi^0$ system for $0.029 \leq t \leq 0.3$ $(GeV/c)^2$, with $\Delta(1236)$ events removed. Combined data from all five beam momenta. Curve shown is peripheral phase space, normalized to the data below 1000 MeV but outside the 700 to 900 MeV region.

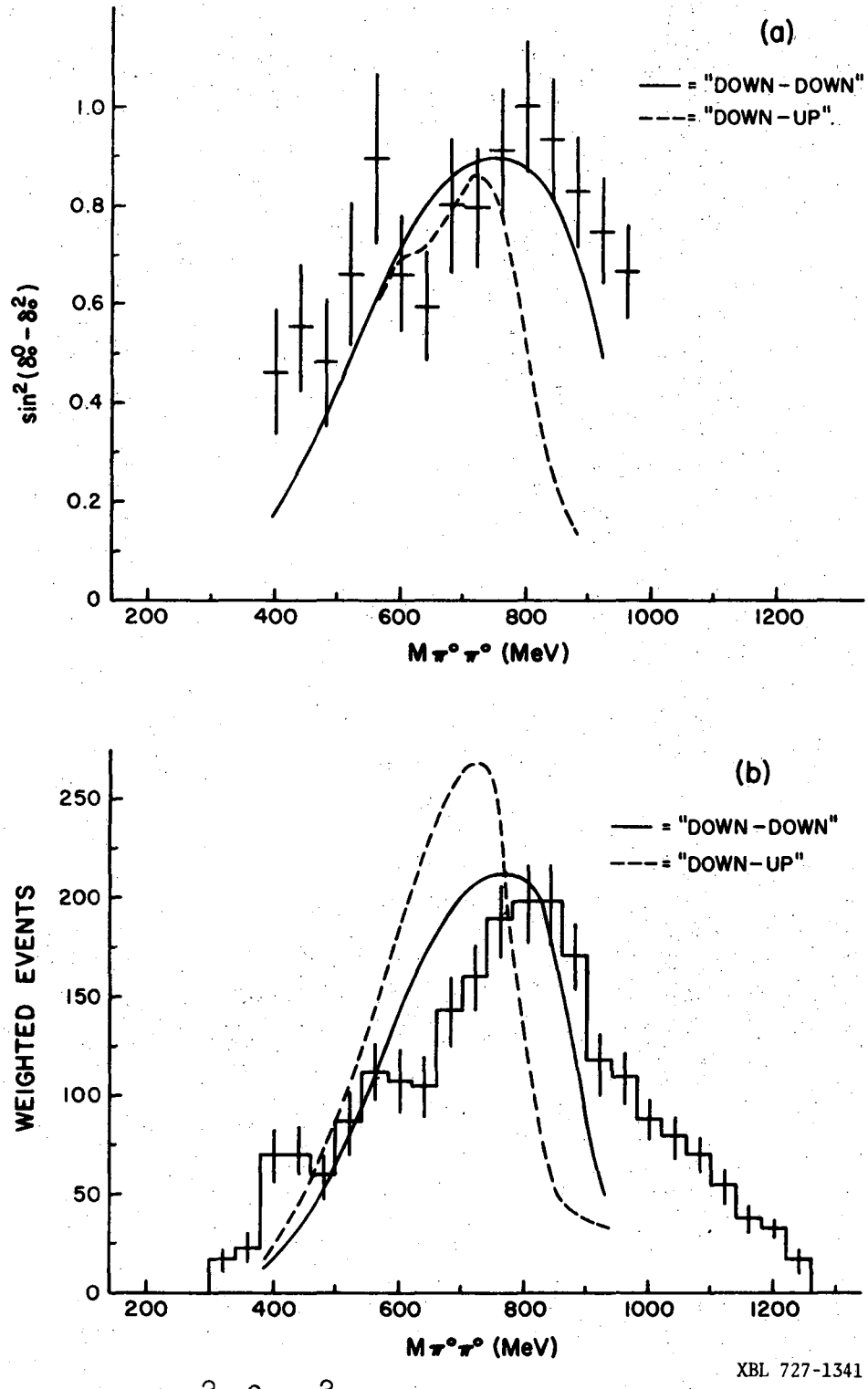

Fig. 8. (a) $\sin^2(\delta_o^o - \delta_o^2)$ as a function of the dipion mass; (b) mass spectrum of the dipion system. The data sample for both plots consists of events with $0.029 \leq t \leq 0.3$ $(GeV/c)^2$. In plot (b), events in the $\Delta(1236)$ mass band have been excluded. Combined data from all momenta. The curves shown are the predictions of the phase-shift solution of Protopopescu et al.[28] for δ_o^o and Baton et al.[29] for δ_o^2. The normalization of the curves in (b) is described in the text.

TECHNICAL INFORMATION DIVISION
LAWRENCE BERKELEY LABORATORY
UNIVERSITY OF CALIFORNIA
BERKELEY, CALIFORNIA 94720